PRAMANA
— journal of
physics

Vol. 59, No. 1
July 2002
pp. 53–68

Beam optics of the folded tandem ion accelerator at BARC

S SANTRA and P SINGH
Nuclear Physics Division, Bhabha Atomic Research Centre, Mumbai 400 085, India
Email: ssantra@apsara.barc.ernet.in

MS received 6 October 2001; revised 30 January 2002

Abstract. The beam optics of the 6 MV folded tandem ion accelerator, that has recently been commissioned at Bhabha Atomic Research Centre, Mumbai, is presented. Typical beam trajectories for proton and ^{12}C beams under different conditions, are shown. The constraints on the design due to the use of the infrastructure of the Van de Graaff accelerator, which existed earlier, are discussed.

Keywords. Folded tandem ion accelerator; beam optics; matrix formalism.

PACS Nos 29.27.Eg; 41.85.Ar; 41.85.Qg

1. Introduction

The increasing interest in heavy ion accelerated beams for use in multidisciplinary researches of Bhabha Atomic Research Centre envisaged the need to convert the single stage 5.5 MV Van de Graaff accelerator (that existed in our laboratory) into a 6 MV folded tandem ion accelerator (FOTIA). Out of several Van de Graaff accelerators existing in the world, only few of them have been converted into folded tandem accelerators [1,2]. The FOTIA can deliver ion beams of mass up to 40, and energy up to 66 MeV (for a charge state of 10^+ and maximum terminal voltage of 6 MV). Such a facility [3], capable of providing a variety of particle beams, will be used for research in both basic and applied sciences.

The configuration of the FOTIA (figure 1) was worked out by the detailed beam dynamics study. Trajectory calculations were made for different ions at terminal voltages of 1–6 MV, and the optimized design parameters of the various beam handling components were obtained. The use of the pressure tank and the terminal dome of the model CN Van de Graaff accelerator existed earlier in the laboratory put severe constraints on the design parameters. The main restriction was due to the limited acceptance of the 180° magnet (that could be accommodated inside the dome), where the magnet pole gap is kept at 15 mm to allow a field of 1.4 T. The wall thickness of 2.5 mm of the vacuum chamber (with 0.5 mm gap between chamber and pole) reduces the acceptance of the pole gap to 9 mm. The centre-to-centre distance between high and low energy accelerating tubes is 610 mm, and hence, the injector and the analyzing magnets with 90° bend could not be kept side by side on the ground floor as their coils and supporting structure interfered. To avoid this, the

90° bend in the injection line was achieved by a 70° bending magnet and a 20° electrostatic deflector, which added to the difficulty in alignment of the extra axis.

In FOTIA, the negative ions produced (from the cathode sample) by cesium sputtering, are extracted and pre-accelerated up to 150 keV. The singly charged negative ions selected through the 70° magnet are injected into the low energy accelerating tube through the 20° electrostatic deflector. The electrostatic quadrupole triplet and the einzel lens focus the beam to match its parameters to the acceptance of the low energy accelerating tube. The negative ions are accelerated to the positively charged high voltage (up to 6 MV) terminal and lose some of the electrons while passing through the foil stripper (that is kept inside the terminal dome) to become positive ions. The positive ions of particular charge state are bent through the 180° folding magnet, and then again accelerated through the high energy accelerating tube to the ground potential. The diverging beam at the exit of the high energy accelerating tube is focused by the magnetic quadrupole triplet, and then analyzed by the 90° bending magnet. The analyzed beam is guided to the scattering chamber through the second magnetic quadrupole triplet and the switching magnet.

The optics design of FOTIA is discussed in §2. The design parameters of the individual components are discussed in §3. The summary and conclusions are given in the §4.

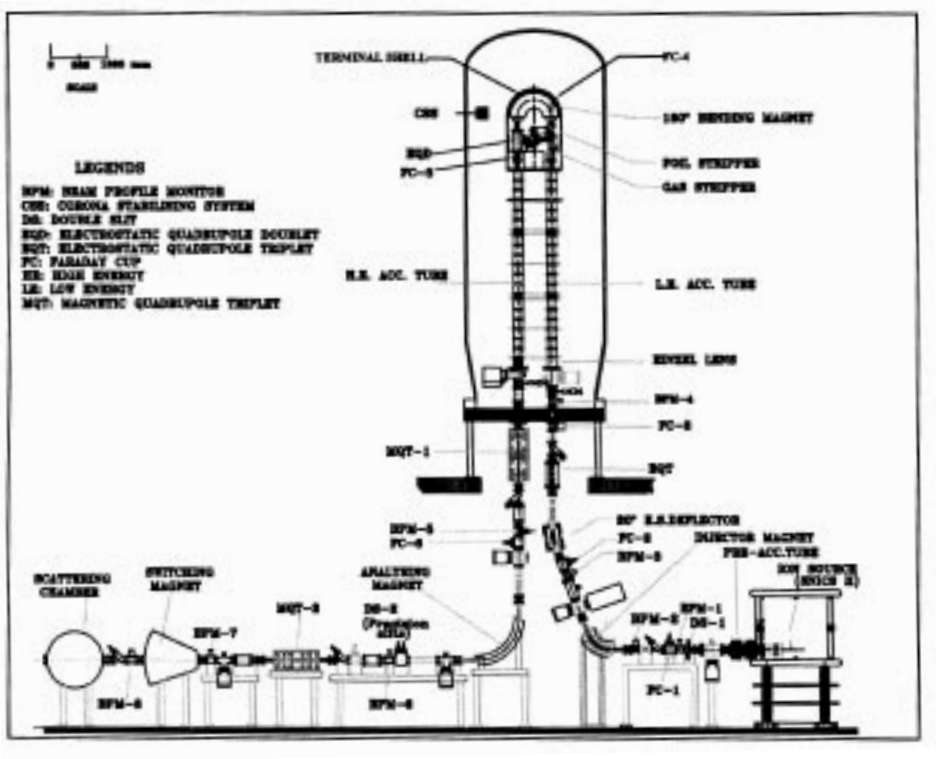

Figure 1. Schematic assembly of the 6 MV folded tandem ion accelerator at BARC.

2. Optics design

In the beam optics study, matrix methods were used to find the displacement and angular divergence of a particle leaving a beam handling component in terms of the corresponding input conditions by linear simultaneous equations. The coefficients of these equations depend on the physical parameters (i.e., length, aperture, etc.) of the transport elements and the electrical power (i.e., voltage and current) applied to them. The behavior of many beam transport elements can be obtained by considering only the first order terms in the dynamics [4]. This yields differential equations with linear solutions. However, in the present study, for some of the components like accelerating tube, einzel lens, etc., the behaviors were obtained by using the empirical relations for the focal lengths that include all the higher order terms. For the remaining components like dipole and quadrupole lenses, since the air gaps between the poles are generally small, the effect of the higher order aberrations could be neglected to simplify our calculations.

Consider a system in which the output displacement and divergence x_2 and x_2' of a particle are given in terms of its input displacement and divergence x_1 and x_1' by equations

$$x_2 = a_{11}x_1 + a_{12}x_1', \qquad x_2' = a_{21}x_1 + a_{22}x_1'. \tag{1}$$

In matrix notation this becomes

$$\begin{pmatrix} x_2 \\ x_2' \end{pmatrix} = \begin{pmatrix} a_{11} & a_{12} \\ a_{21} & a_{22} \end{pmatrix} \begin{pmatrix} x_1 \\ x_1' \end{pmatrix}. \tag{2}$$

Using the above matrix formalism for each component, typical envelopes of the proton and carbon beams at terminal voltages of 2, 4 and 6 MV are shown in figures 2–4. The beam coming out of the ion source is assumed to be circular with a radius of 0.75 mm, a divergence of 180 mrad, and an energy of 1.5 keV. Hence, the ion source emittance is taken to be $\simeq 5.23\pi$ mm mrad MeV$^{1/2}$, in view of the commercially available SNICS-II ion source. The profile of the proton beam, both in X- and Y-plane, from ion source to the foil stripper, is given in figure 2. In this low energy section, since the singly charged negative ions that are selected through the injector magnet pass through only electrostatic components, the profile is assumed to be similar for the ions of other masses. From the stripper to the target in the scattering chamber, the beam profiles of proton and $^{12}C^{4+}$ are shown in figures 3 and 4, respectively. Here, the increase in divergence of the beam after passing through the stripper is also incorporated.

In the three figures 2–4, the dash–dot horizontal line at a height labeled zero in the vertical axis corresponds to the beam axis. It divides the vertical axis into two planes (X-plane and Y-plane). The plane below (above) the beam axis represent the X-plane (Y-plane). The modulus of the negative (positive) value of the vertical coordinate represents the beam size across X-plane (Y-plane). The distance between two thick solid horizontal lines (parallel to the central beam axis) represents the aperture of the accelerating tube, which is 25.4 mm. The lengths of these thick lines are equal to the length of the low/high energy accelerating tube.

As can be seen from these figures, there is no beam loss inside the accelerating tubes for the terminal voltage varying from 2 to 6 MV. While optimizing the parameters at $V_T = 6$ MV, the einzel lens (EL) and the electrostatic quadrupole doublet (EQD) were not required. However, at $V_T = 2$ and 4 MV, they were used for better transmission.

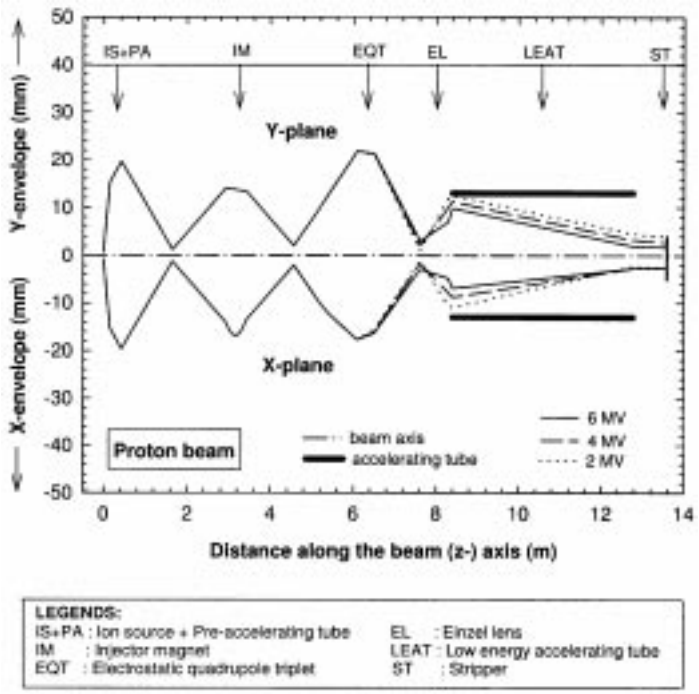

Figure 2. Typical envelopes of the proton beam from ion source to foil stripper in X- and Y-planes with terminal voltage, $V_T = 2$ MV (dotted line), 4 MV (dashed line), and 6 MV (thin solid line). Beam direction is from left to right along the Z-axis. The acronyms with arrows on the top of the plot show the positions of different optical components as explained in the box below the graph.

To obtain full transmission through the accelerator by matching the beam parameters with the acceptance of the low energy accelerating tube, particularly at the terminal voltage of 1–4 MV, it was found necessary to have an einzel lens at the entry of this accelerating tube. A high voltage (up to 75 kV) is applied to the central electrode of an equivalent three tube einzel lens and its end electrodes are grounded. At $V_T = 2$ and 4 MV, the voltages applied to the einzel lens were $V_{EL} = 62$ and 45 kV respectively. The effect of the einzel lens at $V_T = 4$ MV, can be seen in figure 5, where the calculations are made for the proton beam without (dotted line) and with (thin solid line) the voltage applied to the lens. The situation is worse in case of $V_T < 4$ MV.

After the beam passes through the foil stripper, the divergence increases by a large factor due to small angle scattering of the heavy ions from the thin carbon foil. The modified emittance of the beam (particularly of heavier ions and at lower terminal voltages), will not match the acceptance of the 180° magnet which is very small, and hence only part of the beam will pass through. The use of a gas stripper in these conditions will be able to reduce the value of the rms scattering angle. The equivalent thickness of the gas stripper, and hence the scattering angle, can be controlled by changing the gas pressure inside the gas canal. In view of this, arrangements have been made to incorporate a gas stripper inside the terminal, positioned just before the foil stripper.

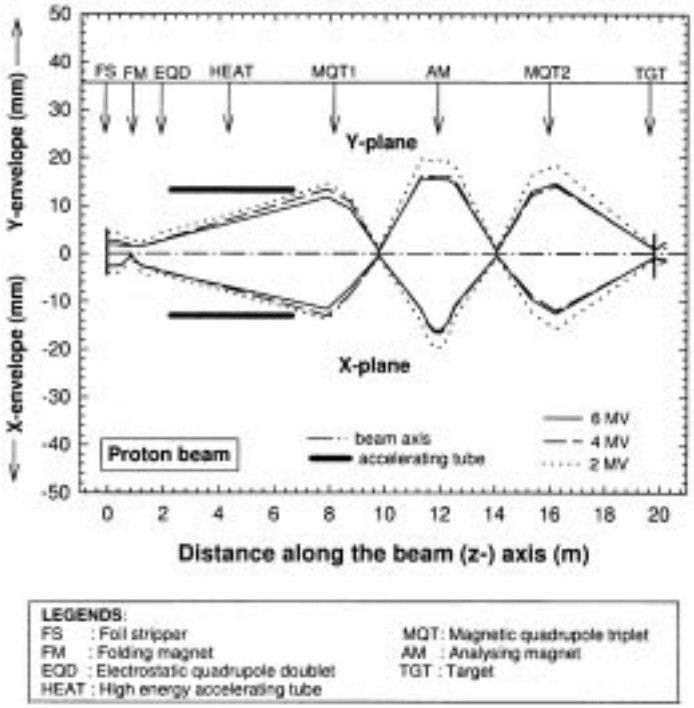

Figure 3. Same as figure 2, but the envelope is from foil stripper to the target in the scattering chamber, where the change in the beam emittance after passing through the foil stripper is incorporated.

The difficulty in obtaining good transmission through the folding magnet is demonstrated in figures 6a and 6b. The parameters of all the components, including those of the einzel lens and the EQD, were also optimized in these calculations. Typical proton beam sizes in both X- and Y-planes, from foil stripper to the exit of the electrostatic quadrupole doublet, are shown in figure 6a. The horizontal axis of the graph represents the relative positions of the stripper, folding magnet and EQD, as marked in the figure. Thick solid lines represent the aperture boundaries for stripper, magnet and EQD. The aperture boundaries of the magnet in two planes are not equidistant from the beam axis because the rectangular vacuum chamber of the folding magnet with effective opening of 19 mm$\times$9 mm allows the maximum beam sizes of $\pm$9.5 mm and $\pm$4.5 mm in X- and Y-planes respectively. Two thin solid lines (close to the beam axis) represent the envelope for the proton beam in X- and Y-planes at $V_{\mathrm{T}} = 6$ MV. Similarly, the dashed and the dotted lines correspond to $V_{\mathrm{T}} = 4$ and 2 MV respectively. The corresponding beam sizes for $^{12}C^{4+}$ are shown in figure 6b. It can be observed that at higher terminal voltages, $V_{\mathrm{T}} = 4$ and 6 MV, both proton and $^{12}C^{4+}$ beam pass through the 180° magnet without an intensity loss. But, at $V_{\mathrm{T}} = 2$ MV, in the case of $^{12}C^{4+}$, the beam is lost after hitting the boundaries and the loss inside the 180° magnet was estimated to be about 25% assuming uniform density distribution in the transverse cross section of the beam. However, there is no loss for proton (H^+) beam in the

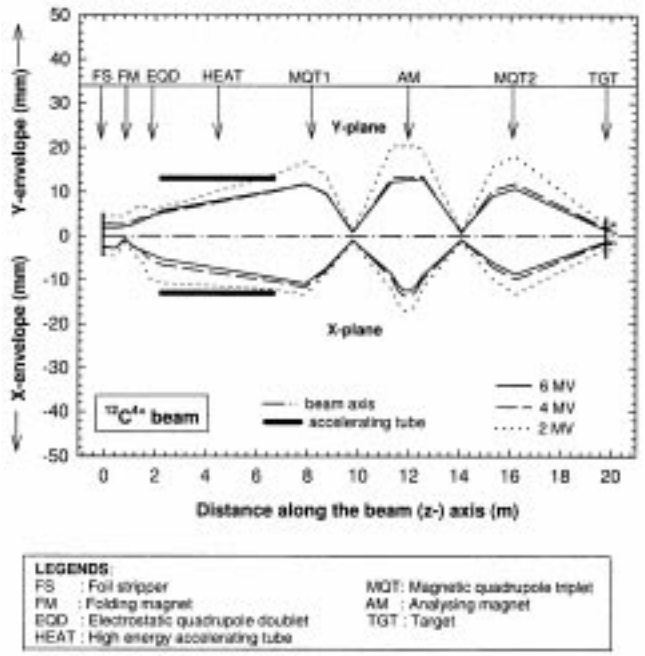

Figure 4. Beam envelopes of the $^{12}C^{4+}$ ion from foil stripper to the target in the scattering chamber in X- and Y-planes with terminal voltage, $V_T = 2$ MV (dotted line), 4 MV (dashed line), and 6 MV (thin solid line). The change in emittance after the stripper is included.

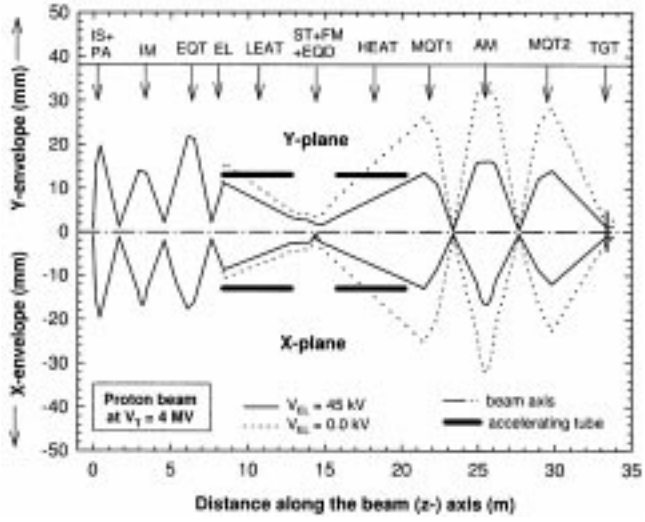

Figure 5. Proton beam envelopes from ion source to the target kept in the scattering chamber, in X- and Y-planes at $V_T = 4$ MV with the einzel lens 'ON' (thin solid line) and 'OFF' (dotted line).

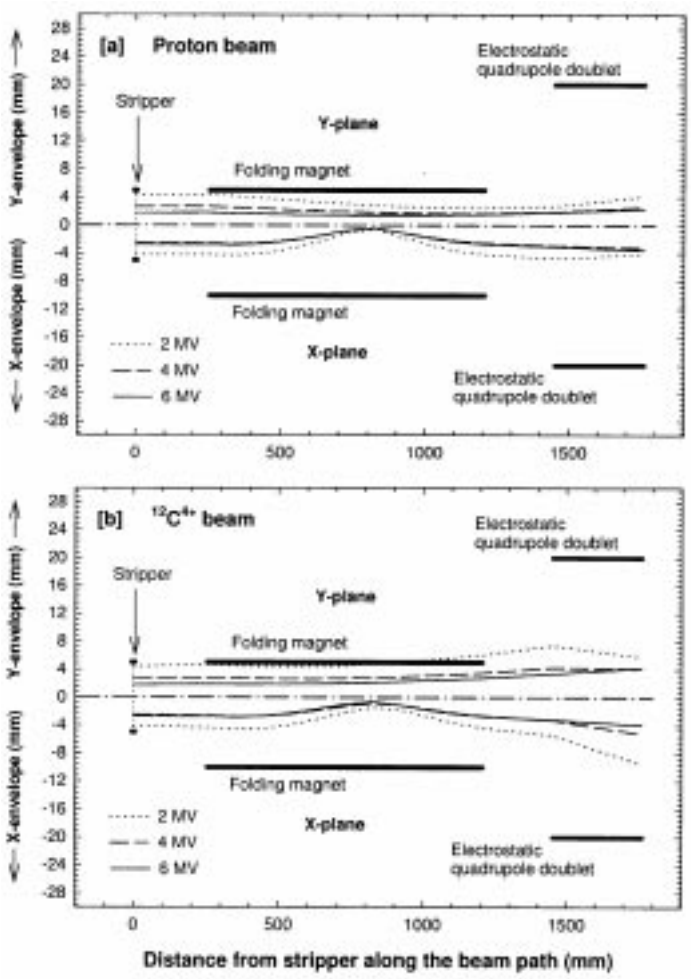

Figure 6. Beam envelopes inside the 180° magnet at $V_T = 2$ MV (dotted line), 4 MV (dashed line) and 6 MV (thin solid line) in X- and Y-planes for (**a**) proton and (**b**) $^{12}C^{4+}$ ions (see text for details).

above condition. It was found that the transmission of heavier ions (with $A \geq 4$) through the present 180° magnet would not be 100% at lower terminal voltages (≤ 3 MV), when the foil is used as stripper. At $V_T = 3$ MV, the transmission loss is $\simeq$14%. However, for proton beam there is no loss at $V_T \geq 2$ MV. A small cutting of the proton beam by the boundary end of the 180° magnet, at $V_T = 1$ MV, is found to reduce the transmission by $\simeq$8%.

The beam coming out of the folding magnet is diverging in both dispersive and non-dispersive planes. An electrostatic quadrupole doublet (EQD) has been incorporated between the 180° magnet and the high energy accelerating tube to match the beam parameters with the angular acceptance of the high energy accelerating tube [5]. This is necessary at

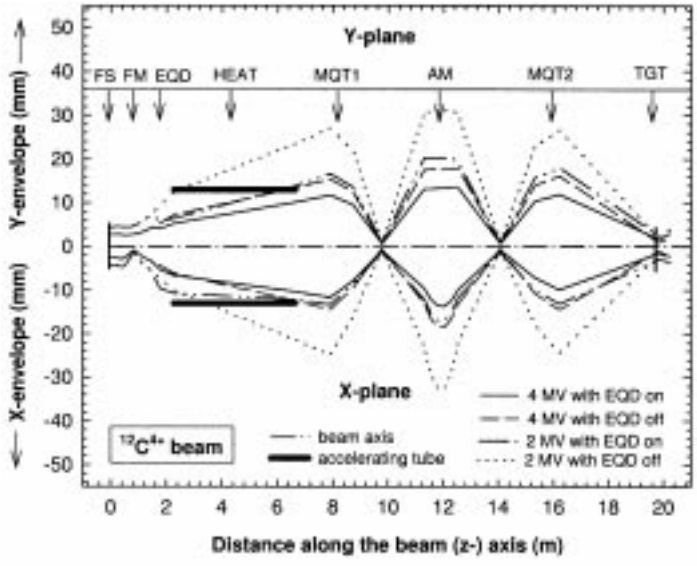

Figure 7. Profile of the $^{12}C^{4+}$ beam starting from the foil stripper and ending at the target kept in the scattering chamber at $V_T = 2$ MV and 4 MV with EQD of the terminal 'ON' and 'OFF'.

the terminal voltages of $V_T \leq 4$ MV, in order to avoid any interception of the beam by the accelerating tube. In figure 7, the beam shapes for $^{12}C^{4+}$ ions from foil stripper to the scattering chamber at $V_T = 2$ and 4 MV are shown with the EQD kept 'ON' (solid line) and 'OFF' (dotted line). It shows how the beam is cut by the accelerating tube when the doublet is switched off.

The details of the design parameters of various optical components are given in the next section.

3. Design details

3.1 *Low energy section*

The low energy section of the FOTIA consists of the components starting from ion source up to the exit of the low energy accelerating tube. The main components in this section are: negative ion source, pre-acceleration tube, 70° injector magnet, 20° electrostatic deflector, einzel lens, electrostatic quadrupole triplet, and low energy accelerating tube. The quality of the beam from the accelerator depends upon the design parameters of the above components, particularly, the ion source emittance, the field uniformity of the injector magnet, the pre-acceleration voltage, and the einzel lens characteristics.

3.1.1 *Ion source*: In FOTIA, the ions, required for injecting into the low energy acceleration tube, are extracted from the source of negative ions by cesium sputtering (SNICS). The ion

source having emittance smaller than the acceptance of the low energy accelerating tube was chosen. The low energy tube acceptance for a waist at the stripper is given by

$$A_{\mathrm{LE}} = \pi \frac{r_1 r_2}{L} \sqrt{\left[1 - \left(\frac{r_2}{r_1}\right)^2\right]} \left[\frac{1}{2}\left(\sqrt{E}_{\mathrm{T}} + \sqrt{E}_{\mathrm{I}}\right)\right] \tag{3}$$

where $r_1 = 12.7$ mm, the tube aperture radius; $r_2 = 4.5$ mm, the foil stripper radius; $L = 4.1$ m, the distance from the entry of the accelerating tube to the foil stripper; $E_{\mathrm{T}} = 1$–6 MeV, the energy of the ion at the terminal; and $E_{\mathrm{I}} = 150$ keV, the injection energy. So, $A_{\mathrm{LE}} \simeq 7.5$–$18.5\pi$ mm mrad MeV$^{1/2}$ corresponding to $E_{\mathrm{T}} = 1$–6 MeV. And when the gas stripper with canal aperture of 6 mm is in position, the value of A_{LE} gets restricted to 6.3–12.8π mm mrad MeV$^{1/2}$ for the above range of the terminal voltage. Therefore, the SNICS-II model of the source having an emittance of $\sim 5\pi$ mm mrad MeV$^{1/2}$, which is less than A_{LE} calculated above, is used in FOTIA. This source can produce ion beams of all elements which form stable negative ions.

3.1.2 *Pre-accelerating tube*: Since the negative ions having loosely bound electrons in their outer shells have a large probability of loosing the electrons during the collisions with the residual gas molecules present in the injection system, it is necessary that they spend minimum time in the beam line before reaching the low energy accelerating tube. Thus higher injection energy is desirable to reduce the beam losses. Also, it is necessary that the beam should have a waist at the stripper and its size (diameter) be ≤ 5 mm while passing through the gas canal having aperture of 6 mm. This requires a magnification of ≤ 1 and thus the injection voltage should be higher. On the basis of the beam optics calculations it was decided that the negtive ions extracted from the ion source would be accelerated up to 150 keV by the pre-accelerating tube. The pre-accelerating tube consists of two sections, each rated for 75 kV. The field in the tube is defined by demountable potential distribution rings. Potential grading for each section is provided by ten 150 MΩ resistors in series over a length of 24.4 cm. A waist is desired at a distance of 785 mm from the end of the tube, that can be obtained by varying the voltage of the extractor and the einzel lens of the ion source, depending on the voltage applied to the pre-accelerating tube and the cathode of the source.

3.1.3 *70° magnet*: The pre-accelerated beam is analyzed by the 70° dipole magnet which is designed and fabricated indigenously. Out of all negative ions extracted from the ion source, the singly charged negative ions of particular mass are selected for injection into the low energy accelerating tube. The magnet has a bending radius of 40 cm and is designed for the maximum magnetic field of 1.4 T in the pole gap of 4 cm. It can bend the ions having mass-energy product $(\mathrm{ME}/q^2) \leq 15$. The pole face of the 70° magnet has been tapered in order to avoid the saturation, and the geometry has been optimized by the computer simulation code 'TRIM' [6] in order to achieve the field uniformity within ±0.1%.

The magnet is designed for focusing in both dispersive and non-dispersive planes. The pole faces were rotated by 19.35° on either side in order to match the object and image points of the magnet in both the planes. The point of double focusing, l''_d, is given by [7]

$$l''_d = \frac{1}{2}\left[\tan(\phi - \psi) - \frac{1}{\phi - \cot\eta}\right] \tag{4}$$

with

$$\tan\psi = \tan\alpha_1 + \frac{1}{l'}, \qquad \tan\eta = \tan\alpha_1 - \frac{1}{l'}, \tag{5}$$

where ϕ, α_1 and l' are angle of deflection, entrance pole rotation and object distance (normalized to the bending radius) respectively. For this magnet, $l' = 3.2$, and $\alpha_1 = 19.35^\circ$.

Thus, considering an object distance of 128 cm (that was required to accommodate the beam diagnostic components), the image distance of the magnet can be found as 103 cm. The image distances in both horizontal ($l''_{\rm h}$) and vertical planes ($l''_{\rm v}$) are calculated separately using the relations [7]

$$\frac{1}{l''_{\rm h}} = \tan(\phi - \psi) - \tan\alpha_2, \qquad \frac{1}{l''_{\rm v}} = \tan\alpha_2 - \frac{1}{\phi - \cot\eta} \tag{6}$$

and are found to be the same as the above value. Here α_2 is the exit pole rotation. A magnet was fabricated and installed in the beam line. The performance of the injector magnet was found to be satisfactory [8] with the measured absolute field and its uniformity matching with the design values.

3.1.4 *20° electrostatic deflector*: The analyzed beam from the 70° magnet is further bent by 20°, with the bending radius of 71.6 cm, using an electrostatic deflector. Two deflecting plates (∼25 cm long, 7 cm wide, and ∼1.2 cm thick) are mounted 3 cm apart inside a vacuum chamber. The electric field **E** required to bend the ions of charge q along the bending radius R, is given by

$$\frac{mv^2}{R} = q\mathbf{E}, \tag{7}$$

where the kinetic energy, $\frac{1}{2}mv^2$ = 150 keV (maximum), R, the bending radius = 71.6 cm, and $q = 1e$. So, the required electric field E is equal to 4.19 kV/cm (maximum). Since the separation between the two deflecting plates is 3 cm, the required voltage will be 12.57 kV.

3.1.5 *Electrostatic quadrupole triplet*: To focus the diverging beam and match the beam parameters to the acceptance of the low energy accelerating tube, an electrostatic quadrupole triplet has been incorporated after the 20° deflector. The four elements of the first singlet are physically identical to those of the third singlet, and also have the same voltage on the elements in the same median plane. The mid elements are rotated by 90° with respect to the end elements in order to obtain the focusing effect in both the planes. The quadrupole triplet of overall length 42.5 cm has the aperture radius of 3.2 cm. The length of the end and mid elements and the separation are $l_{\rm e} = 11.4$ cm, $l_{\rm i} = 15.4$ cm, and $S = 1.5$ cm, respectively.

In the design of the quadrupoles, no force is needed for the particles moving in the central trajectory, but more and more force is required for the particles away from the central trajectory. A constant gradient of field ($\partial E_x/\partial x$ and $\partial E_y/\partial y$), that produces the required force, can be obtained when four poles are hyperbolic in shape. The effective focal length of three quadrupoles including two drift spaces can be calculated using the product of the standard transfer matrices [4]. For a typical ion beam of energy 150 keV,

when a voltage of 10 kV (maximum) is applied to each of the quadrupole elements, the focal length in the converging-diverging-converging plane is ∼82 cm. Usually, the voltage required to the elements of this lens are in the range of 4.0 to 6.0 kV.

3.1.6 *Einzel lens*: The focusing properties of an electrostatic three-electrode 'single' lens are discussed in [9]. The characteristics of the einzel lens used in our system is shown in figure 8 where power of the lens (D/f) is plotted as a function of the ratio of the voltage applied to the middle electrode (V_{EL}) to the voltage corresponding to the beam energy (V_i). The aperture diameter (D) in our case is equal to 56 mm. The maximum voltage required for the einzel lens is 75 kV.

3.1.7 *Low energy accelerating tube*: The entrance to the low energy accelerating tube behaves as a strong converging lens. Fringing fields dominate the beam optics of electrostatic accelerating tubes. Wherever the field changes, a single-aperture type of lens appears [10]. The effect is pronounced where the fields rise from zero at the entrance (converging lens) and return to zero at the exit (diverging lens) of a normal accelerating tube. To a first approximation, the focal length of an aperture lens (a single circular aperture in a plane electrode separating two regions of different electric field) is given by [11]

$$f = \frac{4V_{\mathrm{i}}}{E_1 - E_2} = \frac{4V_{\mathrm{i}}}{\Delta E}, \tag{8}$$

where V_{i} is the potential corresponding to the ion energy. E_1 and E_2 are the fields preceding and following the aperture. A more realistic focal length may be obtained as [12]

$$f = \frac{4\xi V_{\mathrm{i}}}{\Delta E}, \tag{9}$$

where ξ, the aperture correction factor given by [13],

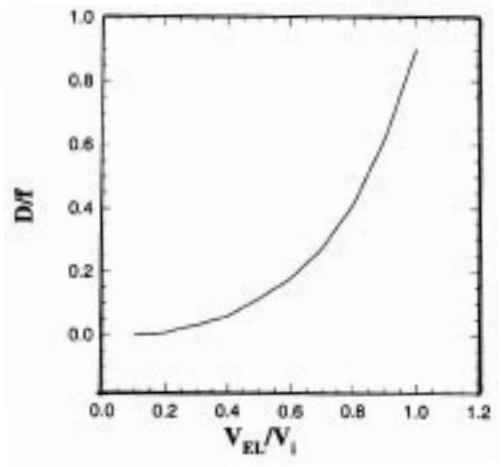

Figure 8. Einzel lens characteristics obtained in terms of focal length normalized to aperture (D/f) as a function of voltage applied to the lens (which is also normalized to the voltage corresponding to injection energy i.e. $V_{\mathrm{EL}}/V_{\mathrm{i}}$).

$$\xi \approx a + b\frac{D}{f}. \tag{10}$$

Here a and b are constants of values $a \simeq 1.0$ and $b \simeq 0.57$, and D is the aperture diameter of the accelerating tube.

For the present case, a realistic formula has been used to find out the focal length which is given as

$$f = \frac{1}{\Delta E}[2V_{\mathrm{i}} + (4V_{\mathrm{i}}^2 + 2.28V_{\mathrm{i}}D\Delta E)^{1/2}]. \tag{11}$$

If the beam enters the tube with initial energy 150 keV and terminal voltage vary from 1 to 6 MV, then, the focal length of the low energy accelerating tube can be found to vary from 1900 mm to 340 mm. At low terminal voltage, one can reduce the incident energy to adjust the focal point slightly. But too much of reduction of incident energy is not allowed due to the reasons mentioned earlier. Hence, the einzel lens which is incorporated just before the entry of the tube would be very helpful to adjust the combined focal length by its variable voltage. The calculations showed that with einzel lens in operation it is possible to achieve a good transmission for terminal voltage from 1 to 6 MV.

3.2 *Terminal section*

The main optical components inside the terminal are 180° magnet, electrostatic quadrupole doublet and foil stripper. Due to the limited space inside the terminal dome, these components had to be very compact, and no beam profile monitor could be accommodated.

3.2.1 *Stripper*: When the beam passes through the stripper foil, there is significant increase in divergence of the beam due to small angle scattering of heavy ions in thin foils. A reasonable description is obtained by using a mean square scattering angle given by [14]

$$\langle \phi^2 \rangle = 0.25 \left[\frac{Z_{\mathrm{s}}(Z_{\mathrm{s}}+1)}{A_{\mathrm{s}}}\right] \frac{Z_{\mathrm{i}}^2}{E_{\mathrm{i}}^2} L, \tag{12}$$

where ϕ is the scattering angle in mrad, L the foil thickness in μg/cm^2, Z_{s} the atomic number of the stripper material, A_{s} the mass number of the stripper material, Z_{i} the atomic number of the incident ion and E_{i} the incident ion energy in MeV.

In FOTIA we use carbon foil of $\sim$5 μg/cm^2 as stripper. Defining a parameter θ_{s}, the scattering angle may be written as

$$\langle \phi^2 \rangle = \theta_{\mathrm{s}}^2 L, \tag{13}$$

where L is the length of the stripper. Applying to ray trace formalism, if we consider individual rays then it is more appropriate to consider linear rather than quadratic addition to the coordinate vector. For a ray with its position and divergence being characterized by x and θ, the transformation will be

$$\begin{pmatrix} x \\ \theta \end{pmatrix} = \begin{pmatrix} x_0 \\ \theta_0 \end{pmatrix} + \theta_{\mathrm{s}} \begin{pmatrix} L^{3/2}/\sqrt{6} \\ L^{1/2}/\sqrt{2} \end{pmatrix}. \tag{14}$$

Since L is very small, there will be no appreciable change in size x. However, the angle θ will expand suddenly and become $\theta_0 + (\theta_s L^{1/2}/\sqrt{2})$. The resulting increase in phase space area occupied by the beam is minimized by keeping the spot size as small as possible.

When the gas stripper is used instead of foil stripper, the thickness L can be reduced in order to reduce the divergence, especially for heavier masses and lower terminal voltages. A typical pressure of 3×10^{-3} torr of N_2 gas over a length of 500 mm gas canal (of aperture 8 mm) would be equivalent to about 0.2 μg/cm^2 thickness [15], which reduces the root mean square scattering angle to one-fifth.

3.2.2 *180° magnet*: The indigenously designed and fabricated folding magnet bends the positive ion beams by 180°. The magnet was accommodated inside the terminal dome. As the centre-to-centre distance between the high and low energy accelerating tubes is 61 cm, it restricts the bending radius of the magnet to 30.5 cm only. The magnetic field of maximum 1.4 T can be obtained inside the pole gap of 15 mm with field uniformity of $\pm$0.15% over the pole width of 25 mm. Although, the rigidity of this magnet is small due to small bending radius, the ions of mass up to 40 can still be bent because the values of their mass-energy products are small as they acquire high charge states after passing through the stripper.

As mentioned earlier, the acceptance of this magnet is poor and part of the beam is lost in its vacuum chamber. To optimize the matching of the acceptance of the 180° magnet to scattered beams from the foil, the entrance pole of the magnet is set to focus in the dispersive (deflection) plane of the magnet. The magnet entrance pole was required to be rotated by an angle of 13.3° for optimized beam transmission. Pole face rotation also reduces the divergence in the non-dispersive plane. With the focal point at the foil position, particles scattered from a point in the foil would form more or less a small sized parallel beam between the magnet poles. A waist is formed when the beam has traversed 120°, whereas with a parallel beam incident on a normal pole tip the cross over would be at 90°. An exit pole angle of 4.1° was also required to reduce the divergence in the vertical plane.

The reason why a magnetic dipole is preferred to an electrostatic one for 180° bending is as follows: (a) The beam with different charge states after passing through the stripper will strike the poles on either side except a particular charge state whose trajectory matches the central path of the magnet. When the defocused charges strike the poles they flow to the ground without disturbing the magnetic field whereas, in electrostatics, it is very difficult to maintain a constant field between the two poles when a large amount of variable beam current with different charge states are falling on either of the electrodes. (b) The electrostatic deflector is also not preferred to avoid sparks between the two electrodes as the voltage gradient required for an electrostatic deflector is sometime quite high ($\sim$ 133 kV/cm) and sensitive to the vacuum which might go bad due to the beam striking on the electrodes and the stripper. Frequent sparks in the transport line may lead to a vacuum breakdown in the entire accelerator.

3.2.3 *Electrostatic quadrupole doublet*: Design principle of the EQD is exactly the same as that of the EQT, except that here there are two quadrupoles instead of three. The aperture was kept at 40 mm. The lengths of the two elements and the separation between them are 140 mm and 30 mm respectively. For a typical $^{12}C^{4+}$ beam, a voltage of 0–10 kV is required for the quadrupole elements when the terminal voltage is in the range of 2–6 MV.

3.3 *High energy section*

The optical elements of this section are: high energy accelerating tube, magnetic quadrupole triplet, and analyzing magnet. The positively charged ions coming out of the high voltage terminal get accelerated towards the ground potential, and then get focused and analyzed by the magnetic quadrupole triplet and the analyzing magnet respectively.

3.3.1 *High energy accelerating tube*: The high energy accelerating tube has a converging lens effect at the entrance which ordinarily is much weaker than that described earlier for the low energy stage. The focal length decreases with increasing charge state. For a circular aperture, the approximate focal length is $f \simeq 4l/q$, where l is the active length of the high energy acceleration stage, q is the charge state of the ions, and the injection energy is ignored as usually it is very small as compared to the total energy.

3.3.2 *Magnetic quadrupole triplet*: The accelerated beam leaving the high energy accelerating tube is diverging and is focused by a magnetic quadrupole triplet placed after the high energy accelerating tube. It can focus ions with mass-energy product (ME/q^2) up to 50. The focal point of the quadrupole is the object point of the 90° analyzing magnet. The pole shapes of the magnetic quadrupoles are similar to that of the electrostatic quadrupoles. The lengths of the end element, the mid element and the distance of separation between two quadrupoles are $l_e = 0.112$ m, $l_i = 0.182$ m and $S = 0.178$ m respectively. The aperture diameter of the triplet is 77.2 mm. The focal length of this lens, when a maximum field gradient of 10.5 T/m is applied on the ion beam of ME/$q^2 = 50$ is calculated to be 99 cm. The typical field gradient required for proton and carbon beams is in the range of 3.5–7.6 T/m. The performance of the indigenously built MQT was found to be satisfactory when tested with the beam.

3.3.3 *Analysing magnet*: An indigenously built double focusing dipole magnet with deflection angle of 90^o has been used to analyze the beam. The beam of particular mass and charge state that is already selected by the 180° magnet is energy analyzed by this magnet. The magnet has a bending radius of 75 cm and designed for the maximum magnetic field of 1.4 T in the pole gap of 4 cm. It can bend the ions having mass-energy product (ME/q^2) ≤ 50.

A pole face geometry similar to 70° magnet was followed in the case of the 90° magnet. The dimensions have been optimized to achieve the field uniformity within ±0.1%. The magnet is designed for focusing the beam in both dispersive and non-dispersive planes. The standard pole face rotation of 26.5° on either end of this magnet was set in order to obtain the object and image distance of 2ρ, where ρ is the effective bending radius (i.e., 77 cm).

4. Summary and remarks

The complete beam optics of the FOTIA was worked out and the design of the entire accelerator was finalized. Despite stringent constraints due to space limitations, the optimized design of the accelerator will be able to provide beams of various ions of up to $A \simeq 40$ at a

terminal voltage up to 6 MV. Although the transmission for the lighter ions like proton and alpha at 6 MV terminal voltage was found to be almost 100%, it is not the case for heavier ions and at lower voltages. The poor acceptance of the 180° magnet and the limited space availability due to the use of high voltage terminal and accelerator tank of the old Van de Graaff accelerator, are the main constraints in the optics design to obtain high transmission. An einzel lens at the entry of the low energy accelerating tube, and a quadrupole doublet at the exit of the 180° magnet inside the terminal dome, were introduced to obtain better transmission (particularly at low terminal voltages, $V_T \leq 4$ MV, and for heavier ions) through the 180° magnet and the high energy accelerating tube, respectively. A gas stripper assembly is also being incorporated in the terminal that will be used (instead of the foil stripper) in order to reduce the divergence of the beam, by reducing the equivalent stripper thickness, which in turn will increase the transmission for heavier beams at lower terminal voltages.

The beam optics calculations have been tested with the successful acceleration of $^{12}C^{4+}$ beam and the measurement of Rutherford back scattering (RBS) from gold, tin and iron targets, that is used to characterize the beam from the FOTIA [16]. A typical RBS spectrum for the system $^{12}C+^{197}Au$ is shown in figure 9, where the falling edge of the spectrum at the highest energy was taken as the scattered energy of the RBS from the front surface. Accordingly, the incident energy was calculated from the kinematics.

Although there are several difficulties in folded tandem accelerator compared to a straight one, the former has some merits over the latter. First, the size of the whole accelerator is much less, as the column length is reduced by half of that required in case of a straight tandem accelerator. Secondly, the ion source being on the ground floor, the access

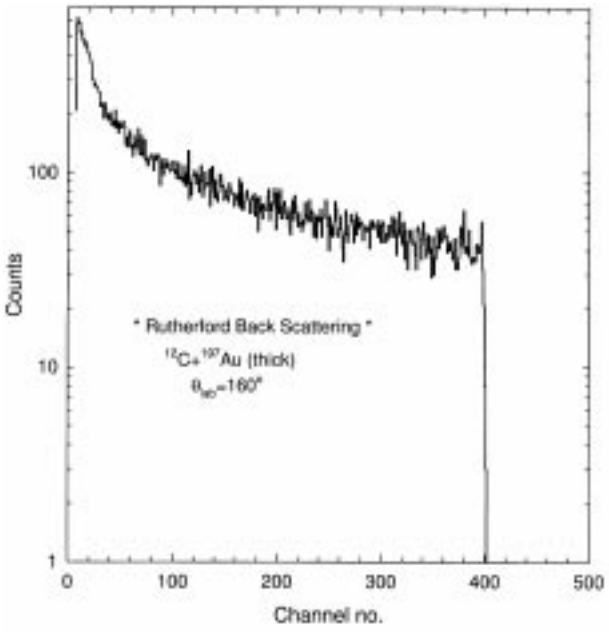

Figure 9. Typical RBS spectrum for $^{12}C+^{197}Au$ at energy ~ 12 MeV.

to the deck for changing cathode sample, etc., and controlling their parameters by local console are easier. Lastly, the most important one is, the sensitivity to the mass energy selection for accelerator mass spectrometry (AMS) studies is superior because of its extra dipole (folding) magnet in the terminal.

Acknowledgements

We thank Shri V A Hattangadi and P Surendran for their help in the initial stage of the calculations. We express our deep sense of gratitude to all the members of the FOTIA section for their contributions towards setting up the facility and characterizing the beam. Thanks are also due to A Kakodkar, S S Kapoor, B K Jain and S Kailas for their incessant encouragement during this work.

References

[1] H Naylor, *Nucl. Instrum. Methods* **63**, 61 (1968)
[2] P J S B Barrat, T R Brock, G Doucas, T J L Greenway, A Henwood, A R Homes, H R McK Hyder, A B Knox, G M Parker and J Takacs, *Nucl. Instrum. Methods* **184**, 9 (1981)
[3] P Singh, *Indian J. Pure Appl. Phys.* **35**, 172 (1997); **39**, 4 (2001)
[4] A P Banford, *The transport of charged particle beams* (Spon, London, 1966)
[5] S Santra and P Singh, *Proc. DAE Nucl. Phys. Symp. (India)* **B42**, 404 (1999)
[6] J S Colonias, *Particle accelerator design: Computer programs* (Academic Press, New York and London, 1974)
A M Winslow, *J. Comput. Phys.* **1**, 149 (1966)
[7] W G Cross, *Rev. Sci. Instr.* **22**, 717 (1951)
[8] S Santra, P Singh, H R Mittal, E Shallom, M J Kansara, P J Raut, R V Patkar, S P Sarode, N Fernandes, Rajesh Kumar, M Y Vaze, S K Gupta, A Agarwal and B K Jain, *Proc. DAE Nucl. Phys. Symp. (India)* **B40**, 472 (1997)
[9] O Klemperer, *Electron optics* (University Press, Cambridge, 1953)
[10] V K Zworykin *et al*, *Electron optics and the electron microscope* (J Willey, New York, 1945)
[11] C J Davisson and C J Calbrick, *Phys. Rev.* **38**, 585 (1931); **42**, 580 (1932)
[12] M M Elkind, *Rev. Sci. Instrum.* **24**, 129 (1953)
[13] P J Stenning and C W Trowbridge, Reading University/Rutherford Laboratory Report RU/RL-1 (1968)
[14] T Joy, *Nucl. Instrum. Methods* **106**, 237 (1973)
[15] Anders Wiebert, Bengt Erlandsson, Ragnar Hellborg, Kristina Stenström and Göran Skog, *Nucl. Instrum. Methods* **A364**, 201 (1995)
[16] P Singh, P V Bhagwat, S K Gupta, S Santra, M J Kansara, A Agarwal, Rajesh Kumar, E Shallom, A K Gupta, R V Patkar, P Sapna, S P Sarode, N B V Subrahmanyam, P J Raut, S C Ojha, B K Jain and S S Kapoor, *Proc. Int. Nucl. Phys. Symp. (India)* **B43**, 522 (2000)